Vitrification of Thin Polymer Films: From Linear Chain to Soft Colloid-like Behavior

ARTICLE *in* MACROMOLECULES · MARCH 2015

Impact Factor: 5.8 · DOI: 10.1021/ma502556n

6 AUTHORS, INCLUDING:

Alexandros Chremos
National Institute of Standards and Technology
30 PUBLICATIONS **270** CITATIONS
SEE PROFILE

Georgios Sakellariou
National and Kapodistrian University of Athens
58 PUBLICATIONS **605** CITATIONS
SEE PROFILE

David W. Gidley
University of Michigan
183 PUBLICATIONS **4,247** CITATIONS
SEE PROFILE

Peter F Green
University of Michigan
93 PUBLICATIONS **1,586** CITATIONS
SEE PROFILE

Macromolecules

Article

pubs.acs.org/Macromolecules

Vitrification of Thin Polymer Films: From Linear Chain to Soft Colloid-like Behavior

Emmanouil Glynos,[†,‡] Bradley Frieberg,[‡,§] Alexandros Chremos,[#] Georgios Sakellariou,[%] David W. Gidley,[∥] and Peter F. Green*[,†,‡,⊥]

[†]Department of Material Science and Engineering, [‡]Bionterfaces Institute, [§]Department of Macromolecular Science and Engineering, [∥]Department of Physics, [⊥]Department of Chemical Engineering, University of Michigan, Ann Arbor, Michigan 48109, United States

[#]Department of Chemical Engineering, Centre for System Process System Engineering, Imperial College, South Kensington Campus, London SW7 2AZ, U.K.

[%]Department of Chemistry, University of Athens, Panepistimiopolis, Zografou, 15771 Athens, Greece

ABSTRACT: We show that the vitrification of star-shaped polystyrene (PS), of functionality f and molecular weight per arm M_w^{arm}, thin films supported by silicon oxide, SiO_x, is strongly dependent on M_w^{arm} and f. When f is small, the vitrification behavior is similar to that of linear-chain PS where the average glass transition, T_g, decreases with decreasing film thickness ($\Delta T_g < 0$). However, for sufficiently large f and small M_w^{arm}, T_g becomes independent of film thickness ($\Delta T_g \approx 0$). In this region, where $\Delta T_g \approx 0$, the star-shaped macromolecules self-assemble into ordered, periodic structures, similar to that of soft spheres or colloids, as revealed by simulations and experiments. This is identified as the soft-colloidal region. The transition from the linear-chain-like to the soft-colloidal-like region occurs over an intermediate range of functionalities and arm lengths; throughout this transition range $\Delta T_g > 0$. We show that the overall vitrification behavior of these thin film star-shaped polymers is due to competing entropic interactions associated with changes in f and M_w^{arm}. The vitrification behavior of thin star-shaped PS films on SiO_x is summarized in terms of a "diagram of states".

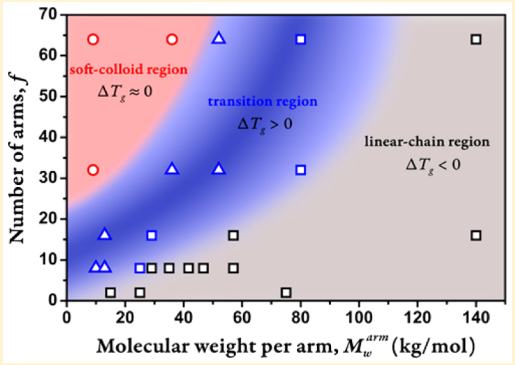

INTRODUCTION

The function and reliability of diverse technologies, from sensors and actuators to energy storage/conversion and information storage, rely on an understanding of the structural and dynamical properties of polymers at the nanoscale. When macromolecules are confined to nanoscale dimensions, entropic effects and interactions between the chain segments and the external interfaces influence the structure of the polymer such that it deviates the bulk, over certain length scales.[1−3] Changes in the local free volume, organizational order, and segmental mobilities are natural consequences of confinement. Of particular interest in this paper is the glass transition of thin films of star-shaped polymers.

Investigations of the effects of geometrical confinement on the glass transition of thin polymer films have largely focused on linear chains.[1−9] The effects are generally manifested in films with thicknesses H on the order of tens of nanometers, where the average glass transition temperature, $T_g(H)$, deviates from the one in bulk, T_g^{bulk}. For linear chain free-standing films, $T_g(H)$ decreases with decreasing H, $\Delta T_g < 0$ ($\Delta T_g = T_g(H) - T_g^{bulk}$). A macromolecule located at an unconstrained free surface experiences an enhancement in its configurational freedom (increase in local free volume), and therefore increased local mobility, with respect to a chain in the bulk.[4,10−13] In fact, it has been shown that the local T_g at the free surface $T_g^{surface} < T_g^{bulk}$.[14,15] In the case of linear polymer films supported by nonwetting surfaces, such as polystyrene (PS) on silicon oxide (SiO_x) substrates, $\Delta T_g < 0$.[14,15] This behavior is influenced primarily by effects due to the free surface, not by the effects of the comparatively weak polymer−SiO_x interactions. On the other hand, when the interactions between the polymer and the substrate are sufficiently strong (e.g., polar interactions), then $\Delta T_g > 0$; the poly(methyl methacrylate) (PMMA)/SiO_x and the poly(tetramethylbisphenol polycarbonate) (TMPC)/SiO_x systems are two of many such examples.[16−18]

The foregoing indicates that changing the substrate would be an effective means by which to change the T_g vs H dependence of a supported polymer film. Recently, we showed that for thin films of star-shaped PS polymers of functionality f and average molecular weight per arm M_w^{arm}, supported by SiO_x substrates, that ΔT_g was a function of f and M_w^{arm}. By varying the functionality from $f = 2$ (linear chain) to $f = 8$, while keeping the molecular weight of each arm length fixed at $M_w^{arm} = 10$ kg/mol, ΔT_g changed from negative to positive.[19] However, for a fixed value of $f = 8$, the polymers behaved like linear chains,

Received: December 18, 2014
Revised: March 5, 2015
Published: March 26, 2015

DOI: 10.1021/ma502556n
Macromolecules 2015, 48, 2305−2312

$\Delta T_g < 0$, when M_w^{arm} was sufficiently large, which is not unexpected.[20,21] $\Delta T_g > 0$ for star-shaped macromolecules is associated with the fact that these branched molecules experience enhanced interfacial attractions compared to their linear analogues, due to the lower entropic penalties they suffer when confined to interfaces.[22−28] In fact, we have shown experimentally that for the star-shaped polymers with $f = 8$ and $M_w^{arm} = 10$ kg/mol the local T_gs at the free surface and at the substrate were greater than the bulk, i.e., $T_g^{surface} > T_g^{bulk}$ and $T_g^{substrate} > T_g^{bulk}$.[19] Moreover, our prior study of the wetting of these branched macromolecules revealed that the macroscopic angle of contact between the polymer and SiO_x substrates decreased by approximately an order of magnitude, when the functionality of the molecule increased from $f = 2$ and $f \sim 8$.[26] This behavior is consistent with the observed enhancements of the glass transition temperatures.

Generally, because of their architecture, the monomer density along each arm of a star-shaped polymer decreases from the core of the molecule toward the free chain end. This is consistent with the fact that the arms are stretched, compared to free linear chains; hence, they suffer a loss of conformational entropy.[20,21,29−32] The monomer density gradient increases with increasing f and/or decreasing M_w^{arm}, leading to increased long-range entropic repulsion between adjacent macromolecules (arms).[30,31] In the limit of sufficiently large f, this behavior has been suggested to be akin to that of soft colloids. Notably, experiments and simulations reveal that star-shaped polymer molecules of sufficiently high f and low enough M_w^{arm} exhibit high degrees of order due to increased intermolecular repulsion.[32−35]

Recently, we reported changes in the wetting properties of the star-shaped polymers resulting from changes in the behavior of star-shaped polymers from linear-chain-like to soft-colloidal-like behavior.[25] Specifically, the macroscopic equilibrium contact angle θ_∞ of star-shaped polymers with $M_w^{arm} \sim 10$ kg/mol decreased with increasing f, reaching a minimum for $f \sim 16$, where θ_∞ was more than an order of magnitude lower than the corresponding of linear polymers, and then increased with further increasing f, reaching a plateau for high f, $f \geq 32$; the value of θ_∞ at the plateau value was about 5 times lower than their linear analogues. Molecular dynamic simulations indicated that this behavior stems primarily from the effect of architecture on the adsorption behavior of these polymers onto weakly adsorbing surfaces. Whereas for small f the entropic attraction to interfaces enhances surface wetting, the increasingly soft-colloidal-like behavior of these molecules with increasing f and the associated entopic repulsion between molecules influences the "packing" of the molecules at the substrate; this suppresses their surface adsorption tendencies. These competing entropic effects result in a minimum in the wettabilities of macromolecules of $f \sim 16$ and $M_w^{arm} \sim 10$ kg/mol.

The transition from linear chain-like behavior to soft-colloidal-like behavior, with increasing f and/or decreasing M_w^{arm}, on the vitrification of polymers in thin films has not been investigated. A natural question would be the following: what would be the effect of the increasing f and/or decreasing of M_w^{arm} on the vitrification of thin films, supported by weakly interacting substrates? To answer this question, we investigated the effect of f and M_w^{arm} on the glass transition temperature of thin film star-shaped PS, with f up to 64 and M_w^{arm} up to 140 kg/mol, supported by SiO_x substrates. On the basis of the values of f and M_w^{arm}, we identified the so-called colloidal limit, characterized by $\Delta T_g \sim 0$, as well as regions where $\Delta T_g < 0$ and $\Delta T_g > 0$. The transitions between these regions each occur over a limited range of values of f and M_w^{arm}. A "diagram of states" was prepared to communicate this behavior.

EXPERIMENTAL SECTION

The characteristics of the star-shaped polymers are reported in Table 1. The star-shaped polymers with $f \geq 8$ were synthesized for this study

Table 1. Star-Shaped Polystyrene Molecular Characteristics

polymer	functionality (f)[a]	M_n^{arm} (kg/mol)[b]	PDI[c]
StarPS-3arm-19K (SPS-3-19K)[d]	3	19	1.09
StarPS-3arm-109K (SPS-3-109K)[d]	3	109	1.04
StarPS-4arm-4K (SPS-4-4K)[d]	4	4	1.03
StarPS-8arm-10K (SPS-8-10K)[d]	8	10	1.03
StarPS-8arm-13K (SPS-8-13K)	8	13	1.03
StarPS-8arm-25K (SPS-8-25K)[d]	8	25	1.03
StarPS-8arm-28K (SPS-8-28K)	8	28	1.02
StarPS-8arm-35K (SPS-8-35K)[d]	8	35	1.02
StarPS-8arm-41K (SPS-8-41K)[d]	8	41	1.03
StarPS-8arm-47K (SPS-8-47K)[d]	8	47	1.03
StarPS-8arm-57K (SPS-8-57K)	8	57	1.02
StarPS-16arm-13K (SPS-16-13K)	17	13	1.02
StarPS-16arm-28K (SPS-16-28K)	15	28	1.02
StarPS-16arm-57K (SPS-16-57K)	15	57	1.01
StarPS-32arm-9K (SPS-32-9K)	32	9	1.03
StarPS-32arm-37K (SPS-32-37K)	32	37	1.03
StarPS-32arm-53K (SPS-32-53K)	32	53	1.01
StarPS-32arm-80K (SPS-32-80K)	32	80	1.01
StarPS-32arm-140K (SPS-32-140K)	32	140	1.01
StarPS-64arm-9K (SPS-64-9K)	64	9	1.02
StarPS-64arm-37K (SPS-64-37K)	64	37	1.01
StarPS-64arm-53K (SPS-64-53K)	64	53	1.01
StarPS-64arm-80K (SPS-64-80K)	64	80	1.01
StarPS-64arm-140K (SPS-64-140K)[d]	64	140	1.01

[a]Functionality, f, determined by the ratio $(M_w)_{star}/(M_n)_{arm}$. [b]From membrane osmometry in toluene at 35 °C. [c]From SEC in THF at 40 °C calibrated with linear PS standards. [d]Purchased from Polmer Source Inc.

by means of anionic polymerization, using high-vacuum techniques.[36,37] The linear chain PS (molecular weights of 13, 25, and 152 kg/mol) were purchased from Pressure Chemical Inc.; the star-shaped PS with $f \leq 4$ and some of the 8-arm star-shaped PS (indicated by superscript e) were purchased form Polymer Source Inc.

Average Glass Transition of Thin Polymer Films by Ellipsometry. The polymer films were prepared from filtered PS/toluene solutions that were spin-coated onto oxidized silicon wafers (Wafer World Inc.); the native oxide layers were 1.5 nm thick. The silicon wafers were cleaned using a UV-ozone process and then rinsed with toluene, prior to spin-coating. All samples were subsequently annealed in vacuum for at least 24 h at temperatures of $T \sim T_g + 40$ °C. The average T_gs of of the supported film were determined by monitoring the thickness of the film as the film was cooled from a temperature, $T \sim 150$ °C, at 1 °C/min, using a variable angle spectrometric ellipsometer (M-2000, J.A. Woollam Co.), equipped with an Instec heating stage. The measurements were performed at a fixed angle of 70°. The thicknesses, $H(T)$, and refractive indicees, $n(T)$, were determined by fitting the acquired ellipsometric angles Δ and Ψ to a Cauchy/SiO_x/Si model over the entire spectral range (wavelength range 400−1700 nm). During the experiments, the heating stage was purged with purified nitrogen gas, in order to maintain an inert atmosphere. The T_gs were identified as the intersection of extrapolated linear fits through the glassy and rubbery

DOI: 10.1021/ma502556n
Macromolecules 2015, 48, 2305−2312

regions of the ellipsometric data. None of the samples exhibited dewetting, throughout this process, as confirmed using atomic force microscopy (AFM) and optical microscopy.

Depth-Profiling Positron Annihilation Lifetime Spectroscopy (PALS). The T_gs of supported films with thickness $H \sim 350$ nm were determined at different depths beneath the free surface using depth-profiled positron annihilation lifetime spectroscopy (PALS).[38,39] Through control of the implantation energy of the positrons, the mean implantation depth was controlled. Two different beam implantation energies of 0.7 and 3.2 keV, corresponding to the mean implantation depths of 16 and 180 nm, respectively, were used in this study. The apparent T_g at each depth was deduced using methods described elsewhere.[38−40]

Molecular Dynamics Simulations. We now briefly describe the methodology of the molecular dynamics (MD) simulations; the procedure is described in a prior publication.[25] We consider a system of $N = 400$ star-shaped polymers. A star-shaped polymer is represented by a spherical core with f attached chains ($f = 2$, 4, 8, and 16); each chain is composed of $M = 10$ beads. We set the diameter of each polymer bead to be of unit length σ; the spherical core radius is $R_c = 0.25\sigma$ for stars with functionalities $f = 4$, 6, 8, and 16. For linear chains, denoted with $f = 2$, the core is of the same size as the beads that compose the arms. Interactions between polymer beads are described by the cut-and-shifted Lennard-Jones potential, with ε and σ as the energy and range parameters, and the cutoff distance $r_c = 2.5\sigma$. The beads along a chain are connected with their neighbors via a stiff harmonic spring, $V_H(r) = k(r - l_0)^2$, where $l_0 = 0.99\sigma$ is the equilibrium length of the spring and $k = 5000\varepsilon/\sigma^2$ is the spring constant. The core−core and core−monomer interactions are modeled as purely repulsive Weeks−Chandler−Andersen[41] with modifications that account for differences between the particle sizes.[42] The energy and interaction range parameter are chosen to be the same for these interactions such that $\varepsilon_{cc} = \varepsilon_{cb} = \varepsilon$ and $\sigma_{cc} = \sigma_{cb} = \sigma$.

Simulations were performed in a rectangular box of dimensions $L \times L \times h$, with periodic boundary conditions in x- and y-directions; the minimum-image convention was applied. The surface was represented by a structureless solid slab with dimensions $L \times L \times l$ and with thickness l, no less than the maximum range of interactions between beads. The dimensions of the surface were always sufficiently large for polymers, which are permitted to assume various conformations in order to avoid interacting with their own periodic images. The simulation conditions ensured that the polymers were at finite densities within the simulation cell.

The thickness of the polymer film was much larger than typical polymer dimensions (as denoted by the radius of gyration, R_g) so that three distinct regions of the concentration profile could be observed: namely, the adsorbed region at the solid interface, the region affected by the free interface, and the middle where the bulk properties are expected to be recovered (Figure 1). An effective bead−surface potential was used[43] based on integrating the Lennard-Jones interactions arising from a homogeneous distribution of sites with the surface, $V(r) = \varepsilon_s[(2/15)(\sigma/r)^9 - (\sigma/r)^3]$, where ε_s controls the strength of the bead−surface attraction. The temperature and the energetic interactions are set so that the polymers would form a film adsorbed on the substrate above T_g.[35] In the course of the simulations no polymer evaporation was observed, suggesting that the polymers were at an equilibrium state.

The simulations were performed by the large-scale atomic/molecular massively parallel simulator (LAMMPS) at Sandia National Laboratories.[44] The mass of particle scales linearly with volume, so that $m_c = R_c^3 m_b$ for the mass of the polymer bead, m_b, and core, m_c. Simulations were performed in the NVT ensemble. Time averaging was conducted for $O(10^8)$ time steps after equilibration. The time step was set to $\delta t = 0.005\tau$, where $\tau = \sigma(m_b/\varepsilon)^{1/2}$ is the unit of time. Temperature is measured in units of ε/k_B, where k_B is Boltzmann's constant. For the purposes of the current work we have chosen $T = 0.55$, which is above the glass transition temperature of Lennard-Jones chains and star-shaped polymers, i.e., $T \simeq 0.4$.[35] For each film, the conformational and structural properties of the molecules were analyzed.

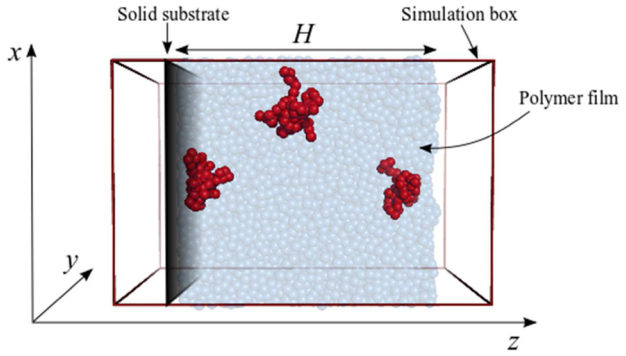

Figure 1. Illustration of a star-shaped polymer film with $f = 8$ and $M = 10$. The polymer beads are rendered transparent except for three star polymers (labeled in red color), which correspond to three possible cases: adsorbed on the solid substrate, in contact with the free interface, and in the middle of the film. The geometry of the simulation box is also presented.

RESULTS AND DISCUSSION

We begin by considering the thickness dependencies of T_g for polymers of varying functionalities f ($2 < f \leq 64$) and comparable arm lengths, $M_w^{arm} \sim 10$ kg/mol. We recently reported that thin films of star-branched PS macromolecules with functionalities $f < 8$, and supported by SiO_x, exhibited average glass transition temperatures that decreased with decreasing film thickness ($\Delta T_g < 0$). However, for macromolecules possessing functionalities of $f = 8$ and $f = 16$, the T_g is enhanced in relation to the bulk, for films in the same thickness range. These data are plotted in Figure 2a. The data in this figure moreover show a new phenomenon: the average T_gs of films of molecules of higher functionalities, $f = 32$ and $f = 64$, remain relatively independent of film thickness. This effect is more clearly illustrated in Figure 2b, where $\Delta T_g(H$=30 nm), the shift of T_g for films of thickness $H = 30$ nm in relation to the bulk, is plotted as a function of f. Notably $\Delta T_g(H = 30$ nm) exhibits a nonmonotonic dependence on f; the magnitude of $\Delta T_g(H = 30$ nm) is largest for $f = 2$ and for $f \sim 8$; beyond functionalities of $f \sim 8$, $\Delta T_g(H = 30$ nm) gradually reaches a limiting value of zero.

This behavior is dependent on the arm length as one might anticipate, since for sufficiently long chains the molecules should behave like linear chains. This point is illustrated in Figure 3a for star-shaped molecules with $f = 8$ and 16: $\Delta T_g(H = 30$ nm) decreases with increasing M_w^{arm} and becomes equal to that of linear PS chains for $M_w^{arm} > 40$ kg/mol. The dependencies of ΔT_g on M_w^{arm} for $f = 32$ and 64 (Figure 3b) is particularly intriguing. For small values of M_w^{arm}, there is no deviation of the average T_g from the bulk, $\Delta T_g \approx 0$. However, ΔT_g exhibits a maximum with increasing M_w^{arm}; with further increasing values of M_w^{arm}, the magnitude of $\Delta T_g(H = 30$ nm) becomes equal to that for linear chains. The location of the maximum occurs at larger M_w^{arm}, for the larger functionality ($f = 64$) star.

The information in the foregoing figures is summarized in Figure 4, in terms of a master plot or "diagram of states", where f is plotted as a function of M_w^{arm}. Three basic regions are evident from this figure: the linear chain regions, where $\Delta T_g < 0$, occurs for molecules of low functionalities and or/high molecular weight per arm (linear-chain region, gray area in

DOI: 10.1021/ma502556n
Macromolecules 2015, 48, 2305−2312

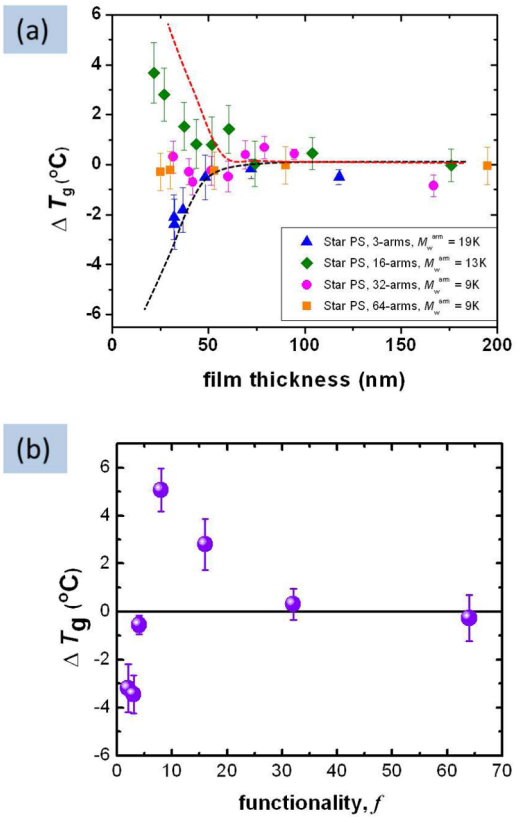

Figure 2. T_gs as a function of film thickness for 3-arm star PS (blue triangles), 16-arm star PS, 32-arm star PS with M_w^{arm} = 9 kg/mol, and 64-arm star PS. The black dashed line and red dashed line corresponds to the T_gs data for a linear PS and an 8-arm with M_w^{arm} = 10 kg/mol as was reported in a previous publication.[19] (b) Effect of the number of arms on the $\Delta T_g(H = 30\ nm) = T_g^{30\ nm} - T_g^{bulk}$.

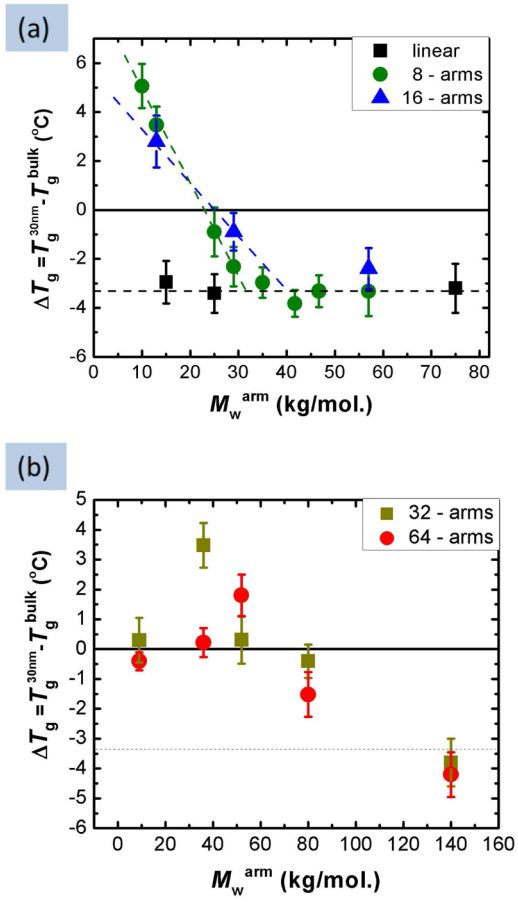

Figure 3. Effect of the molecular weight per arm, M_w^{arm}, on the $\Delta T_g = T_g^{30\ nm} - T_g^{bulk}$ for star-shaped polymers with different functionalities: (a) for linear, 8-arm, and 16-arm star-shaped PS and (b) for 32-arm and 64-arm star-shaped PS. The dashed green and blue lines in (a) are guide line to the eyes, while the black dashed line in both panels corresponds to the ΔT_gs data for a linear PS.

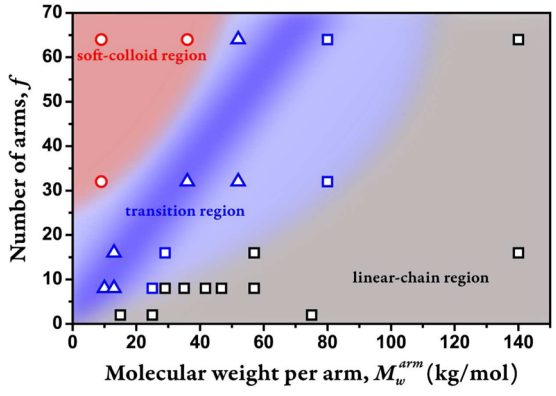

Figure 4. "Diagram of states" for the vitrification behavior of star-shaped polymers: two basic regions are shown here, a linear-chain-like region ($\Delta T_g < 0$) and a new soft-colloidal-like region, ($\Delta T_g = 0$). The transition between them occurs over a range of f and M_w^{arm}.

Figure 4). There is a new region, associated with sufficiently large f and small M_w^{arm}, which we identify as the soft-colloidal region (red area in Figure 4), where $\Delta T_g \approx 0$. The entropic interactions between the molecules and the interfaces are largely exacerbated by the high f and small M_w^{arm}, in contrast to the long arm low f macromolecules. This behavior is akin to that of soft colloids, as briefly discussed above. We will return to this issue later where the outcomes of simulations are discussed. In the meantime, it is worthwhile to briefly consider the physical origins of the third transition region, identified by the blue shaded region in Figure 4. This transition between the soft colloidal-like and linear-chain behavior, where $\Delta T_g > 0$, occurs over a limited range of values for f and M_w^{arm}.

It is well understood and accepted that the interactions between the polymer segments and the external interfaces influence the average T_g of a thin film. Sufficiently thin linear chain PS films supported by SiO_x substrates, which are nonwetting, exhibit average T_gs that are lower than the bulk, $\Delta T_g < 0$, because $T_g^{surface} < T_g^{bulk}$, and the T_g at the substrate is comparable to that of the bulk.[1−3] On the other hand, for linear chain PS supported by gold $\Delta T_g > 0$. This is due to the strong adsorption of linear chain PS molecules on gold surfaces, which has a more dominant effect on the average T_g of the film than the free surface.[14,18] Napolitano and co-workers recently reported a strong correlation between the degree of adsorption and the shifts of T_g in capped thin PS films.[45,46] The enhancements of T_g in relation to the bulk were shown to be linearly proportional to the degree of adsorption, associated with an increase in local free volume at the interfacial regions. As we showed in a recent publication, the adsorption of star-shaped polymers at interfaces is dependent on f.[25] Star-shaped macromolecules experience stronger adsorption on surfaces compared to their linear analogues. This behavior is associated with both an increasing number of monomer in contacts per

DOI: 10.1021/ma502556n
Macromolecules 2015, 48, 2305−2312

molecule with the substrate (enthalpy gain) and a decreasing entropic penalty upon adsorption with increasing f, associated with the gain in free energy. Such interactions would be responsible for enhancing the monomer densities at interfaces, compared to linear chains. The effect increases with increasing f but is eventually suppressed due to crowding (the soft-colloidal region). It is important to note that our prior studies revealed that molecules with these values of f and M_w^{arm} exhibit significantly stronger wetting interactions with the external interfaces than polymers of smaller f and much larger M_w^{arm} as a result of their adsorption behavior on surfaces.[25,26]

With the foregoing in mind, we now report our findings of the interfacial T_gs of the polymers in this study. We investigated the T_g at the free surface, $T_g^{surface}$, using depth-profiling PALS, of PS macromolecules with f = 2 (linear), 8, 16, and 64, each with $M_w^{arm} \sim 10$ kg/mol. Thick films of $H \approx 350$ nm were prepared in order to avoid the influence of the supporting substrate. Two different energies of 0.7 and 3.2 keV of the incident positron beam were used to achieve mean implantation depths of the positron below the free surface of 16 and 180 nm, respectively. The differences between the apparent surface T_g (mean implantation depth of 16 nm) and the T_g of the bulk (mean implantation depth of 180 nm corresponding to the center of the film), $\Delta T_g^{surface} = T_g^{surface} - T_g^{bulk}$, are plotted as a function of f in Figure 5. Whereas $T_g^{surface}$

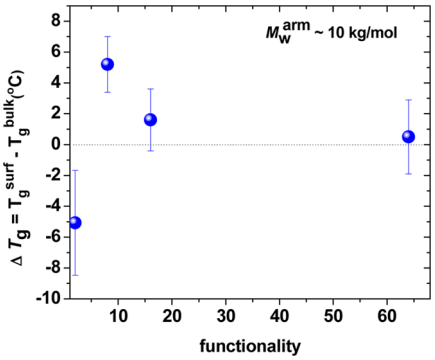

Figure 5. Dependence of $\Delta T_g^{surface}$ (= $T_g^{surface} - T_g^{bulk}$) of f, determined using PALS. $T_g^{surface}$ and T_g^{bulk} were measured at beam energy of 0.7 and 3.2 keV; the corresponding to mean implantation were 16 and 180 nm, respectively.

< T_g^{bulk} for linear-chain PS, $T_g^{surface}$ > T_g^{bulk} for the higher functionality macromolecules of 8 and 16. $\Delta T_g^{surface}$ exhibits a maximum near f = 8, which is consistent with the behavior of ΔT_g. In the case of the sample with the largest f = 64, $\Delta T_g^{surface} \sim 0$. It is notable that for the case of f = 64, where the surface T_g is comparable to the bulk T_g, $T_g^{surface} \sim T_g^{bulk}$, there is no shift in the average T_g of the film for any film thickness studied (Figure 2).

An additional important point that should be considered is the fact that if the T_g has a depth dependence, then different parts of the sample undergo vitrification at different temperatures. This may be examined in detail using ellipsometry. In this regard, an analysis of the breadth of the glass transition, and its changes with film thickness in relation to the bulk, provides information about the local T_g at the external interfacial regions of thin supported films.[15,19,47−49] The thermal expansion $\alpha(T)$ may be extrapolated from the ellipsometric data using the equation

$$\alpha(T) = \frac{H\left(T + \frac{\Delta T}{2}\right) - H\left(T - \frac{\Delta T}{2}\right)}{H_0 \Delta T} \quad (1)$$

where $H(T)$ is the temperature-dependent thickness and experimentally ΔT = 4.2 °C. A stepwise change in $\alpha(T)$ occurs, where this "jump" characterizes the glass transition (Figure 6a). The onset, T^+, and the end of the transition, T^-, of

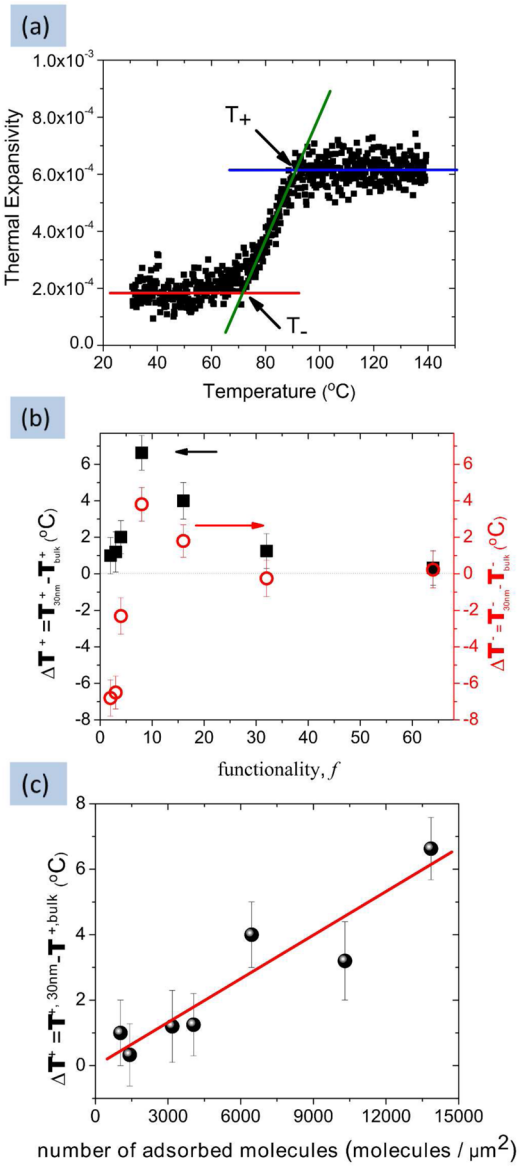

Figure 6. (a) Temperature dependence of the thermal expansion of a 32-arm star-shaped polymer film with H = 95 nm. (b) Plot of ΔT^+ (black solid squares) and ΔT^- (red open circles) as a function of the functionality of the star-shaped polymers. (c) Correlation between ΔT^+ and the variation of the density of the adsorbed polymers for the different systems used in this study.

the glass transition, as measured during cooling, indicate that different regions of the film "fall" out of equilibrium at different temperatures. For thin films, where interfacial regions constitute an increasingly large fraction of the overall material, the quantities $\Delta T^- = T^-_H - T^-_{bulk}$ and $\Delta T^+ = T^+_H - T^+_{bulk}$ manifest differences between the local T_gs, at the interfaces relative to the bulk.[15,19,47]

DOI: 10.1021/ma502556n
Macromolecules 2015, 48, 2305−2312

The dependencies of $\Delta T^{-} = T^{-}_{30\,nm} - T^{-}_{bulk}$ and $\Delta T^{+} = T^{+}_{30\,nm} - T^{+}_{bulk}$ are plotted as a function of f for star-shaped polymers with $M_w^{arm} \sim 10$ kg/mol in Figure 6b. With regard to the dependence of ΔT^{-} on f, its trend is consistent with our conclusions based on the PALS measurements of $\Delta T_g^{surface}$ (Figure 5): ΔT^{-} reflects changes of the local T_g at the free surface, whereas ΔT^{+} is associated with that of the region at the substrate. The dependence of ΔT^{+-} on f is consistent with the ΔT_g (H = 30 nm) vs f (Figure 2b) which show that the ΔT_g in the vicinity of the substrate, $\Delta T_g^{substrate}$, undergoes a maximum at $f \sim 8$, while for large f, $\Delta T_g^{substrate} \approx 0$.

As mentioned above, the extent of interfacial adsorption of the macromolecules influences the local T_g at the vicinity of the substrate. To this end, we determined, experimentally, the number of adsorbed molecules per unit area, ρ_{ads}, and found that ρ_{ads} exhibited a monotonic dependence on f using the same protocol as we used in a recent publication:[25] ρ_{ads} increased with f, reaching a maximum for $f = 8$ and then decreased for $f > 8$. The data in Figure 6c, where ΔT^{+} is plotted as a function of ρ_{ads}, reveal that the shifts in local T_g in the proximity of the substrate (ΔT^{+}) scales reasonably linearly with the degree/strength of adsorption. Earlier we alluded to the notion that the behavior of the system, which for low f is linear-chain-like and eventually becomes soft-colloidal-like, is due to effects associated with two competing entropic effect; the first is the free energy gain due to adsorption (associated with both an increasing number of monomer in contacts per molecule with the substrate and a decreasing entropic penalty upon adsorption), compared to linear chain analogues, and a suppression due to a "crowding effect" (increasing intermolecular entropic repulsion with increasing f). These competing forces can account for the differences on the relative free volume close to the substrate and the corresponding trend of the local T_g at the substrate region with f.

An important outcome of this study is that in the soft-colloid region $T_g^{surface} \approx T_g^{bulk}$; this region is preceded, for smaller f and larger M_w^{arm}, by two other regions where $T_g^{surface} > T_g^{bulk}$ and $T_g^{surface} < T_g^{bulk}$. Deeper insight into the intermolecular interactions that dictate the behavior of these systems may be gleaned from molecular dynamics simulations. As described earlier, thin films composed of molecules with different functionalities, in contact on the one side to a semi-infinite solid substrate and exposed to vacuum on the other side, were considered. The solid substrate is a weakly adsorbing interface: the bead–substrate interactions are slightly more favorable than the bead–bead interactions. At the vacuum interface, the bead–bead interactions are more favorable than the bead–vacuum interactions, i.e., beads exposed to a vacuum do not gain energy. Two types of concentration profiles along the film in the z-direction were constructed; the first profile contains only the polymer particles, while for the second profile only the core particles are considered; the results are plotted in Figures 7a and 7b, respectively. Three regions are apparent from these data; a region in the middle of the film (that can be considered to behave "bulk-like"). The other two regions are at the vicinity of the solid interface ($z/H = 0$) and at free interface ($z/H = 1$).

In the case of linear chains, the bead and core particles profiles are very similar. The characteristic oscillatory behavior is observed at the solid interface with the first peak being the strongest due to the adsorption of molecules on the substrate; this has been reported for other coarse-gained bead–spring[50] or atomistic simulations.[51−53] At the polymer/vacuum interfaces, in contrast, the density decreases with a characteristic sigmoidal

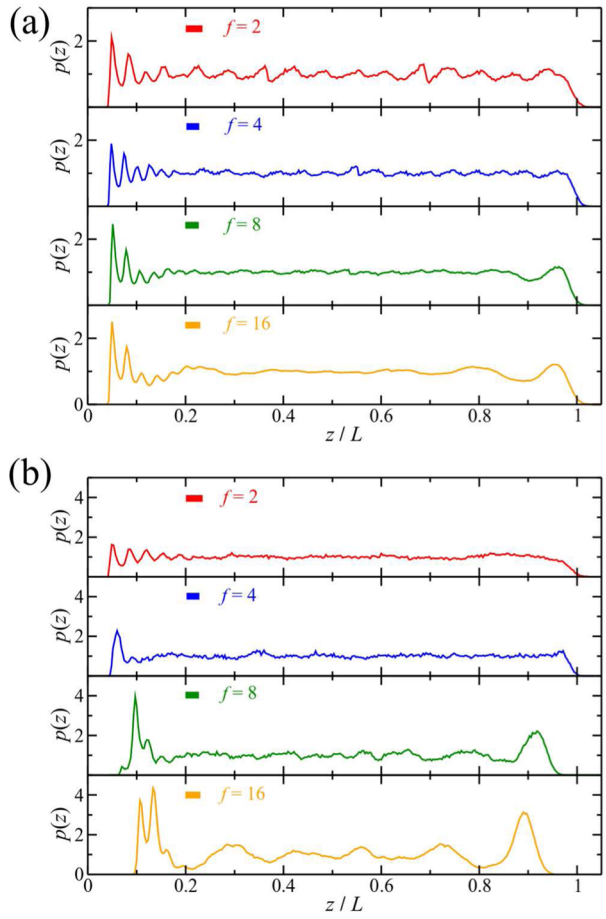

Figure 7. Concentration profiles of star polymer films with M = 10 at different functionalities. Polymer bead (a) and core b) particle concentration profiles are shown here. The profiles representing the functionalities (f = 4, 8, and 16) are displaced vertically.

shape, typical for the free surface of a linear polymer film.[53−55] In star-shaped polymer films the bead concentration is enhanced at both interfaces compared to the bulk; this effect increases with increasing f. This concentration enhancement is stronger at the substrate ($z/H = 0$) due to the strong adsorption behavior of the star-shaped polymers induced by the substrate. However, it is weaker at the film/vacuum interface ($z/H = 1$). The structural changes at the vicinity of the interfaces are more noticeable in the core particle concentration profiles than the bead concentration profiles (compare Figures 7a and 7b). The adsorbed molecules per simulation area, ρ_{ads}, on the substrate were estimated based on the concentration profiles in Figure 7 (data not show here), and the trends with f are in agreement with the experimental data used in Figure 6c and with recently reported molecular simulation data on the adsorption behavior of star-shaped on a substrate from a melt.[25] Linear chains and low functionality star-shaped polymers exhibit no peak at the free interface and at the interior of the film, indicating the free interface does not significantly affect the concentration profile (Figures 7a and 7b). For f = 8, there is a strong peak in the core concentration at the film/vacuum interface (Figure 7b, green line), while such a correlation is lacking at the interior. This indicates a strong positional correlation between the core particles of star-shaped polymer at the vicinity of the free surface. On the other hand, a strong peak in the core concentration at the film/vacuum interface also

DOI: 10.1021/ma502556n
Macromolecules 2015, 48, 2305−2312

occurs for f = 16; there is a positional (oscillatory behavior) correlation in the interior of the film (Figure 7b, yellow line). Computer simulations and experiments have shown that for $f \geq 16$ and with increasing f there is an increasing correlation of the centers of the stars, and ordered structures are formed even in the bulk.[32−34] This behavior is a result of the increasing intermolecular entropic repulsion with increasing f. Nevertheless, the intensity of the oscillatory peaks in the interior is low compared to the one at the film/vacuum interface, indicative of a decreased concentration of star-shaped polymer per unit volume and/or a weaker distance correlation than the film/vacuum interface. Additionally, higher functionalities lead to enhanced repulsion between the stars and an interface (free surface or substrate), leading to an increase of the distance between the core of a star and an interface. This is illustrated in Figure 7b. While the core particle concentration profile is affected by the functionality of the stars, the polymer bead concentration profiles are not. This highlights the notion that a single metric, e.g., monomer concentration profile, is not sufficient to describe the properties of thin film star-shaped macromolecules, which exhibit intramolecular heterogeneity both structurally and dynamically.[35] This will be further investigated in the future.

Our experiments and molecular dynamics simulations reveal that there is a connection between the structure of the star-shaped polymer films (Figure 5), and the changes of the local T_g at the free surface ($\Delta T_g^{surface}$, Figure 5). For stars of f = 8, $\Delta T_g^{surface} > 0$, and the simulations reveal that these macromolecules appear to form ordered structures at the free surface (Figure 7b, green line); a slight enhancement of the monomer density (lower free volume) at the polymer/vacuum interface compared to the bulk (Figure 7b, green line) is also observed. Both the increased monomer density and the ordering of the molecules at the film/vacuum interface would result in a reduction in free volume and hence the observation that $T_g^{surface} > T_g^{bulk}$, i.e., $\Delta T_g^{surface} > 0$. Recall that for a larger functionality of f = 16, $T_g^{surface} > T_g^{bulk}$; in fact, the transition is shown in Figure 5, where $\Delta T_g^{surface}$ is plotted as a function of f. It is also shown in this figure that for much larger functionalities, in the soft-colloidal-like regime, f = 64, the $\Delta T_g^{surface} = 0$.

We investigated the possibility that the macromolecules self-assembled to form ordered structures at the interfaces, as suggested by the simulations (see Figure 7b) of the highest functionality stars. Specifically, we prepared thin films of samples and investigated their topographies using atomic force microscopy (AFM). A typical AFM image of the edge of a 64-arm star-shaped macromolecular thin film, with $M_w^{arm} \sim 10$ kg/mol, is shown in Figure 8. The topography of this film was measured after first scratching it to expose the underlying substrate and annealing it for 1 h at 120 °C. Several steps were formed, and the height of each step corresponded to a length scale of $\sim 2R_g$, indicating the formation of a uniform ordered layers across the film, i.e., self-organization.

CONCLUSION

It is well-known that the average glass transition temperature $T_g(H)$ of a sufficiently thin polymer film of thickness H will differ from the bulk. $T_g(H)$ manifests the effects of local segmental "packing," of chain segments at the interfaces, engendered by the polymer/interface interactions. For linear chain PS molecules, supported by weakly interacting substrates, such as SiO_x, $T_g(H)$ decreases with decreasing film thickness, for films H < 60 nm. This is because the glass transition temperature at the free surface is lower than the bulk, due to the lower free volume, and because the T_g at the substrate is not sufficiently different from the bulk.

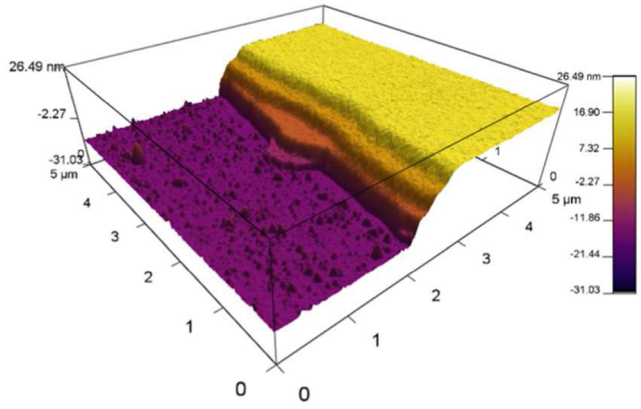

Figure 8. 3D atomic force microscopy image of a scratched/scored of ~35 nm 64-arm with M_n^{arm} = 9 kg/mol star-shaped PS film that was annealed at 120 °C for 1 h.

We showed that the vitrification of polymer thin films composed of star-shaped macromolecules is considerably different from their linear chain analogues. The vitrification behavior is summarized in Figure 4. For smaller values of f, nearly regardless of the arm length, the $T_g(H)$ behavior is virtually identical to that of linear-chain PS ($\Delta T_g < 0$). However, with increasing f and or decreasing M_w^{arm}, the T_g(H) increases in relation to the bulk ($\Delta T_g > 0$). This behavior is associated with an enhancement of the packing of chain segments (decrease in free volume) at both interfaces in relation to the bulk, as shown by simulations. Additionally, the increase in the local T_gs at both interfaces in relation to the bulk are determined experimentally, using ellipsometry and PALS. An interesting phenomenon occurs when f is high and the arms are sufficiently short where $\Delta T_g \approx 0$. In these situations, experiments do not show an excess of segmental packing at the interfaces in relation to the bulk. AFM measurements show evidence of ordered organization of the molecules in the form of layers, in a manner identical to soft spherical particles; steps are observed. The molecular dynamic simulations strongly support this notion of organization. Our results are summarized in terms of a "diagram of states", where the functionality of each molecule is plotted as a function of the arm length.

AUTHOR INFORMATION

Corresponding Author

*E-mail pfgreen@umich.edu (P.F.G.).

Notes

The authors declare no competing financial interest.

ACKNOWLEDGMENTS

Support for this research from the National Science Foundation (NSF), Division of Material Research (DMR-1305749), is gratefully acknowledged.

REFERENCES

(1) Alcoutlabi, M.; McKenna, G. B. *J. Phys.: Condens. Matter* **2005**, *17* (15), R461−R524.

(2) Napolitano, S.; Capponi, S.; Vanroy, B. *Eur. Phys. J. E* **2013**, *36* (6), 37.

DOI: 10.1021/ma502556n
Macromolecules 2015, 48, 2305−2312

(3) Forrest, J. A.; Dalnoki-Veress, K. *Adv. Colloid Interface Sci.* **2001**, *94* (1−3), 167−196.
(4) Baschnagel, J.; Varnik, F. *J. Phys.: Condens. Matter* **2005**, *17* (32), R851−R953.
(5) Lipson, J. E. G.; Milner, S. T. *Eur. Phys. J. B* **2009**, *72* (1), 133−137.
(6) McCoy, J. D.; Curro, J. G. *J. Chem. Phys.* **2002**, *116* (21), 9154−9157.
(7) Mittal, J.; Shah, P.; Truskett, T. M. *J. Phys. Chem. B* **2004**, *108* (51), 19769−19779.
(8) Long, D.; Lequeux, F. *Eur. Phys. J. E* **2001**, *4* (3), 371−387.
(9) Fryer, D. S.; Peters, R. D.; Kim, E. J.; Tomaszewski, J. E.; de Pablo, J. J.; Nealey, P. F.; White, C. C.; Wu, W. L. *Macromolecules* **2001**, *34* (16), 5627−5634.
(10) Forrest, J. A.; DalnokiVeress, K.; Stevens, J. R.; Dutcher, J. R. *Phys. Rev. Lett.* **1996**, *77* (10), 2002−2005.
(11) Morita, H.; Tanaka, K.; Kajiyama, T.; Nishi, T.; Doi, M. *Macromolecules* **2006**, *39* (18), 6233−6237.
(12) Forrest, J. A.; DalnokiVeress, K.; Dutcher, J. R. *Phys. Rev. E* **1997**, *56* (5), 5705−5716.
(13) Torres, J. A.; Nealey, P. F.; de Pablo, J. J. *Phys. Rev. Lett.* **2000**, *85* (15), 3221−3224.
(14) Keddie, J. L.; Jones, R. A. L.; Cory, R. A. *Europhys. Lett.* **1994**, *27* (1), 59−64.
(15) Kawana, S.; Jones, R. A. L. *Phys. Rev. E* **2001**, *63* (2), 021501.
(16) Pham, J. Q.; Green, P. F. *J. Chem. Phys.* **2002**, *116* (13), 5801−5806.
(17) Pham, J. Q.; Green, P. F. *Macromolecules* **2003**, *36* (5), 1665−1669.
(18) Keddie, J. L.; Jones, R. A. L.; Cory, R. A. *Faraday Discuss.* **1994**, *98*, 219−230.
(19) Glynos, E.; Frieberg, B.; Oh, H.; Liu, M.; Gidley, D. W.; Green, P. F. *Phys. Rev. Lett.* **2011**, *106* (12), 128301.
(20) Vlassopoulos, D. *J. Polym. Sci., Part B: Polym. Phys.* **2004**, *42* (16), 2931−2941.
(21) Vlassopoulos, D.; Fytas, G. From Polymers to Colloids: Engineering the Dynamic Properties of Hairy Particles. In *High Solid Dispersions*, Cloitre, M., Ed.; Springer-Verlag: Berlin, 2010; Vol. *236*, pp 1−54.
(22) Striolo, A.; Prausnitz, J. M. *J. Chem. Phys.* **2001**, *114* (19), 8565−8572.
(23) Minnikanti, V. S.; Archer, L. A. *Macromolecules* **2006**, *39* (22), 7718−7728.
(24) Qian, Z. Y.; Minnikanti, V. S.; Sauer, B. B.; Dee, G. T.; Archer, L. A. *Macromolecules* **2008**, *41* (13), 5007−5013.
(25) Glynos, E.; Chremos, A.; Frieberg, B.; Sakellariou, G.; Green, P. F. *Macromolecules* **2014**, *47* (3), 1137−1143.
(26) Glynos, E.; Frieberg, B.; Green, P. F. *Phys. Rev. Lett.* **2011**, *107* (11), 118303.
(27) Kosmas, M. K. *Macromolecules* **1990**, *23* (7), 2061−2065.
(28) Chremos, A.; Camp, P. J.; Glynos, E.; Koutsos, V. *Soft Matter* **2010**, *6* (7), 1483−1493.
(29) Daoud, M.; Cotton, J. P. *J. Phys. (Paris)* **1982**, *43* (3), 531−538.
(30) Likos, C. N. *Phys. Rep.* **2001**, *348* (4−5), 267−439.
(31) Likos, C. N.; Lowen, H.; Watzlawek, M.; Abbas, B.; Jucknischke, O.; Allgaier, J.; Richter, D. *Phys. Rev. Lett.* **1998**, *80* (20), 4450−4453.
(32) Pakula, T. *Comput. Theor. Polym. Sci.* **1998**, *8* (1−2), 21−30.
(33) Pakula, T.; Vlassopoulos, D.; Fytas, G.; Roovers, J. *Macromolecules* **1998**, *31* (25), 8931−8940.
(34) Vlassopoulos, D.; Pakula, T.; Fytas, G.; Roovers, J.; Karatasos, K.; Hadjichristidis, N. *Europhys. Lett.* **1997**, *39* (6), 617−622.
(35) Chremos, A.; Glynos, E.; Green, P. F. *J. Chem. Phys.* **2015**, *142* (4), 044901.
(36) Hadjichristidis, N.; Iatrou, H.; Pispas, S.; Pitsikalis, M. *J. Polym. Sci., Part A: Polym. Chem.* **2000**, *38* (18), 3211−3234.
(37) Uhrig, D.; Mays, J. W. *J. Polym. Sci., Part A: Polym. Chem.* **2005**, *43* (24), 6179−6222.
(38) Xie, L.; Demaggio, G. B.; Frieze, W. E.; Devries, J.; Gidley, D. W.; Hristov, H. A.; Yee, A. F. *Phys. Rev. Lett.* **1995**, *74* (24), 4947−4950.
(39) Hristov, H. A.; Bolan, B.; Yee, A. F.; Xie, L.; Gidley, D. W. *Macromolecules* **1996**, *29* (26), 8507−8516.
(40) DeMaggio, G. B.; Frieze, W. E.; Gidley, D. W.; Zhu, M.; Hristov, H. A.; Yee, A. F. *Phys. Rev. Lett.* **1997**, *78* (8), 1524−1527.
(41) Weeks, J. D.; Chandler, D.; Andersen, H. C. *J. Chem. Phys.* **1971**, *54* (12), 5237.
(42) Sewell, T. D.; Menikoff, R.; Bedrov, D.; Smith, G. D. *J. Chem. Phys.* **2003**, *119* (14), 7417−7426.
(43) Sides, S. W.; Grest, G. S.; Stevens, M. J. K. *Macromolecules* **2002**, *35* (2), 566−573.
(44) Plimpton, S. J. *J. Comput. Phys.* **1995**, *117*, 1.
(45) Napolitano, S.; Wubbenhorst, M. *Nat. Commun.* **2011**, *2*, 260.
(46) Napolitano, S.; Rotella, C.; Wubbenhorst, M. *ACS Macro Lett.* **2012**, *1* (10), 1189−1193.
(47) Kim, S.; Hewlett, S. A.; Roth, C. B.; Torkelson, J. M. *Eur. Phys. J. E* **2009**, *30* (1), 83−92.
(48) Fakhraai, Z.; Forrest, J. A. *Phys. Rev. Lett.* **2005**, *95* (2), 4.
(49) Lan, T.; Torkelson, J. M. *Polymer* **2014**, *55*, 1249−1258.
(50) Yoon, D. Y.; Vacatello, M.; Smith, G. D. *Monte Carlo and Molecular Dynamics Simulations in Polymer Science*; Oxford University Press: New York, 1995.
(51) Xia, T. K.; Jian, O. Y.; Ribarsky, M. W.; Landman, U. *Phys. Rev. Lett.* **1992**, *69* (13), 1967−1970.
(52) Borodin, O.; Smith, G. D.; Bandyopadhyaya, R.; Byutner, E. *Macromolecules* **2003**, *36* (20), 7873−7883.
(53) Daoulas, K. C.; Harmandaris, V. A.; Mavrantzas, V. G. *Macromolecules* **2005**, *38* (13), 5780−5795.
(54) Theodorou, D. N. *Macromolecules* **1989**, *22* (12), 4589−4597.
(55) Mansfield, K. F.; Theodorou, D. N. *Macromolecules* **1991**, *24* (23), 6283−6294.

DOI: 10.1021/ma502556n
Macromolecules 2015, 48, 2305−2312